Three-Dimensional Structure and Interannual Variability of the Kuroshio Loop Current in the Northeastern South China Sea

ZHONGBIN SUN

Physical Oceanography Laboratory/IAOS and Frontiers Science Center for Deep Ocean Multispheres and Earth System, Ocean University of China, Qingdao, China

ZHIWEI ZHANG

Physical Oceanography Laboratory/IAOS and Frontiers Science Center for Deep Ocean Multispheres and Earth System, Ocean University of China, and Laboratory for Ocean Dynamics and Climate, National Laboratory for Marine Science and Technology, Qingdao, China

BO QIU

Department of Oceanography, University of Hawai'i at Mānoa, Honolulu, Hawaii

XINCHENG ZHANG

Physical Oceanography Laboratory/IAOS and Frontiers Science Center for Deep Ocean Multispheres and Earth System, Ocean University of China, Qingdao, China

CHUN ZHOU, XIAODONG HUANG, WEI ZHAO, AND JIWEI TIAN

Physical Oceanography Laboratory/IAOS and Frontiers Science Center for Deep Ocean Multispheres and Earth System, Ocean University of China, and Laboratory for Ocean Dynamics and Climate, National Laboratory for Marine Science and Technology, Qingdao, China

ABSTRACT

Based on long-term mooring-array and satellite observations, three-dimensional structure and interannual variability of the Kuroshio Loop Current (KLC) in the northeastern South China Sea (SCS) were investigated. The 3-yr moored data between 2014 and 2017 revealed that the KLC mainly occurred in winter and it exhibited significant interannual variability with moderate, weak, and strong strengths in the winters of 2014/15, 2015/16, and 2016/17, respectively. Spatially, the KLC structure was initially confined to the upper 500 m near the Luzon Strait, but it became more barotropic, with kinetic energy transferring from the baroclinic mode to the barotropic mode when it extended into the SCS interior. Through analyzing the historical altimeter data between 1993 and 2019, it is found that the KLC event in 2016/17 winter is the strongest one since 1993. Moored-data-based energetics analysis suggested that the growth of this KLC event was primarily fed by the strong wind work associated with the strengthened northeast monsoon in that La Niña–year winter. By examining all of the historical KLC events, it is found that the strength of KLC is significantly modulated by El Niño–Southern Oscillation, being stronger in La Niña and weaker in El Niño years. This interannual modulation could be explained by the strengthened (weakened) northeast monsoon associated with the anomalous atmospheric cyclone (anticyclone) in the western North Pacific during La Niña (El Niño) years, which inputs more (less) energy and negative vorticity southwest of Taiwan that is favorable (unfavorable) for the development of KLC.

---

1. Introduction

The Kuroshio (i.e., the western boundary current of the North Pacific subtropical gyre), which originates from the North Equatorial Current bifurcation at the east coast of Philippines, transports huge amounts of mass and heat northward to the midlatitudes and plays an important role in modulating the North Pacific climate variability (Qiu and Lukas 1996; Lien et al. 2015; Hu et al. 2015). By the time the northward-flowing Kuroshio passes by the Luzon Strait, a deep gap of ~300 km width between the Luzon Island and Taiwan Island, it tends to bend clockwise and sometimes intrudes into the northeastern South China Sea (NESCS) (Nitani 1972; Shaw 1989; Sheremet 2001; Wu et al. 2016, 2017). Based on multiple satellite observations, previous studies have pointed out that the Kuroshio in the Luzon Strait generally presents three different major states, i.e., loop, leap, and leak states (Caruso et al. 2006; Nan et al. 2011, 2014).[1] Of the three states, the loop state presents an anticyclonic semienclosed flow structure and most of the time it can result in an anticyclonic eddy (AE) shedding in the NESCS (Zhang et al. 2017). Because the eddy shedding can transport substantial amounts of momentum, and warm, salty, and nutrient oligotrophic Kuroshio water into the interior SCS, it strongly modulates the SCS circulation as well as the biogeochemical processes (Xue et al. 2004; Xiu and Chai 2011; Xiu et al. 2016; Zhang et al. 2013, 2017).

The study of Kuroshio loop can trace back to 1970s when Nitani (1972) first reported that "the Kuroshio turns to the northwest and its main axis reaches as far west as 121°E, with a maximum velocity of about 3 kt (1 kt ≈ 0.51 m s^{-1}). One branch often goes westward at 20°N and enters the South China Sea, and most parts of it go around the warm eddy and then return to the main axis of the Kuroshio." After that, the study of Li and Wu (1989, hereafter LW89) pointed out the similarity between the SCS and the Gulf of Mexico and termed the Kuroshio loop state as "Kuroshio Loop" with a reference to the Gulf Stream Loop Current. Subsequent to LW89, many studies have reported the Kuroshio loop event and examined its spatiotemporal characteristics based on different models or datasets. For examples, based on a three-dimensional (3D) nonlinear model, Zhang et al. (1995) proposed that the Kuroshio intruded into the NESCS as a "loop" which can extend westward to 118°E in the surface layer. Through analyzing the hydrographic data, Li et al. (1998) argued that an AE

observed in the NESCS was shed from the Kuroshio loop and its influence depth can reach 1000 m. Based on surface drifter data, Guo et al. (2013) revealed that the maximum latitudinal scale of Kuroshio loop was ~210 km and the westward velocity was greater than the eastward velocity. Recently, the study of Zhang et al. (2017) has directly revealed the horizontal structure of the Kuroshio loop (i.e., westward flow in the middle and eastward flow in the northern portion of the Luzon Strait) using concurrent satellite and moored observations. Although Zhang et al. (2017) acknowledged that the Kuroshio loop is not a stable current, they kept the term Kuroshio Loop Current (KLC) following LW89 given the fact that it can sometimes persist for several months. Furthermore, through reconstructing the 3D thermohaline structure of the AE shed from KLC and analyzing its water mass properties, Zhang et al. (2017) suggested that the eddy shedding event can result in a 0.24–0.38 Sv (1 Sv ≡ 10^6 m^3 s^{-1}) westward volume transport through the Luzon Strait. However, because the previous observations were primarily confined to the upper ocean, the full-depth structure of KLC and how it evolves in the NESCS are still poorly known.

In addition to the spatial structures, seasonal variation of the KLC was also widely studied. At present, many studies have reached a consensus that the KLC primarily occurs in winter and rarely occurs in summer (Wang and Chern 1987; Wu and Chiang 2007; Jia and Chassignet 2011; Nan et al. 2011, 2014; Zhang et al. 2017). For example, through analyzing the historical altimeter data, Zhang et al. (2017) identified a total of 19 prominent KLC and eddy shedding events between October 1992 and October 2014. Among these 19 KLC events, nearly 90% (17 of 19) occurred in winter. The reasons for winter enhancement of the KLC were ascribed to the northeast monsoon (Farris and Wimbush 1996; Centurioni et al. 2004; Wu and Hsin 2012) and the weakened strength of the upstream Kuroshio east of the Luzon Island during the winter season (Sheremet 2001; Sheu et al. 2010; Yuan and Wang 2011).

Compared with its seasonal variation, the KLC's variation on interannual-to-decadal time scales is poorly investigated. In contrast, many previous efforts have been made on the interannual-to-decadal variations of Kuroshio intrusion into the SCS and the Luzon Strait transport. Generally, their variations on interannual and decadal time scales were proposed to be modulated by the El Niño–Southern Oscillation (ENSO) and Pacific decadal oscillation (PDO), respectively, although different studies based on different datasets have drawn diverse conclusions (e.g., Ho et al. 2004; Qu et al. 2004; Song 2006; Wang et al. 2006; Wu 2012; Yu and Qu 2013; Sun et al. 2016). It is worth emphasizing that the Kuroshio intrusion and the Luzon Strait transport are different from the strength of KLC, even though the three

---

[1] "Leap state": when passing by the Luzon Strait, the main body of the Kuroshio flows northward across the Luzon Strait. "Leak state": when passing by the Luzon Strait, a portion of the Kuroshio water flows into the SCS (Nan et al. 2011).
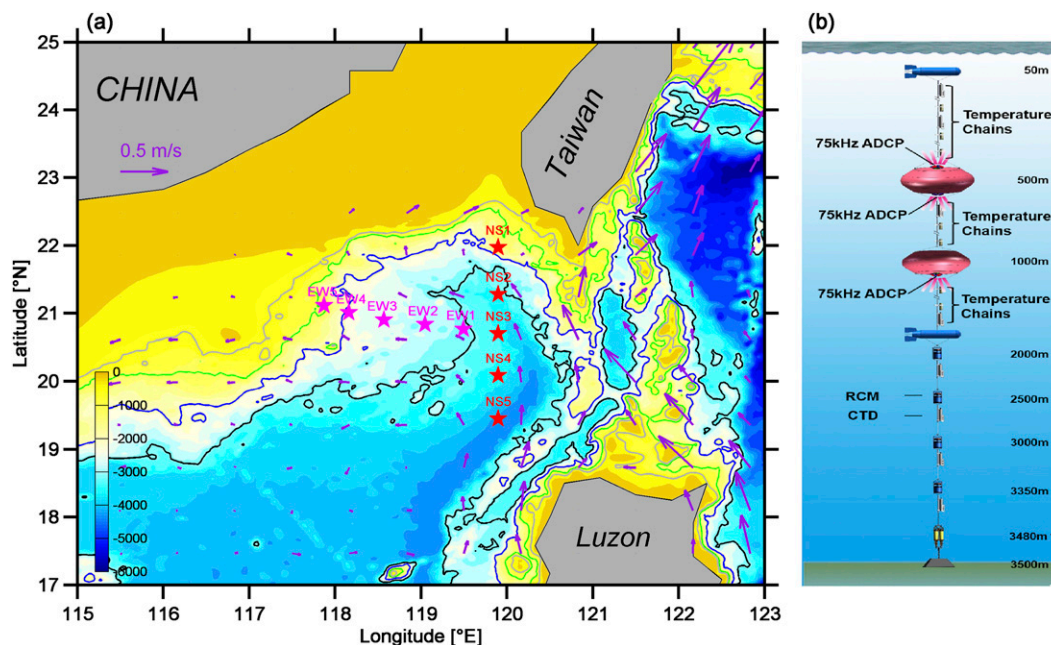
FIG. 1. (a) Locations of the moorings and bathymetry of the NESCS. Red and purple stars denote moorings NS1–NS5 at the NS section and EW1–EW5 at the EW section, respectively. Purple vectors represent the mean surface geostrophic current. Gray, green, blue, and black lines indicate 500, 1000, 2000, and 3000 m isobaths, respectively. (b) A typical schematic diagram of the mooring configuration. The nominal depths of the instruments (i.e., ADCPs, RCMs, CTDs, and temperature chains) are marked in the diagram.

phenomena have some connections. For the Kuroshio intrusion into the SCS, the occurrence of KLC only accounts for less than 20% of the total intrusion state (Nan et al. 2011). With respect to the Luzon Strait transport, it has a sandwich structure in vertical and only its upper-layer component is partially contributed by the Kuroshio intrusion (Tian et al. 2006; Zhang et al. 2015; Gan et al. 2016). As such, the interannual variability of the KLC and its modulation mechanism are to a large degree unclear at present.

Here, based on long-term observations from a mooring array in the NESCS, the full-depth 3D structure and interannual variability of the KLC were investigated in this study. By combing the historical altimeter data and other datasets, mechanisms of the KLC's interannual modulation were also examined. The remainder of this paper is organized as follows. Section 2 describes the data and method we used. Section 3 shows the general spatiotemporal characteristics of the KLC. In section 4, 3D structure of the KLC is examined. In sections 5, interannual modulation mechanism of the KLC is discussed. Finally, the summary is given in section 6.

2. Data and method

a. Moored data

To study the multiscale dynamical processes in the SCS, the SCS mooring array was constructed since 2009,

and the data of which have successfully been used to reveal the spatiotemporal characteristics and the associated dynamics of the internal waves, mesoscale eddies, and deep circulation (e.g., Huang et al. 2016; Zhang et al. 2016; Zhou et al. 2017). As a part of the SCS mooring array, a total of 10 bottom-anchored moorings (section NS: NS1–NS5, section EW: EW1–EW5) were deployed in the NESCS to obtain the nearly full-depth velocity and temperature/salinity (T/S) data between June 2014 and June 2017. The section NS (EW) was along the ~119.9°E longitude (~21°N latitude) west of the Luzon Strait (Fig. 1a). Except for the mooring EW1 (June 2014–June 2015 and June 2016–June 2017), all the other moorings (NS1–NS5, EW2–EW5) were deployed for three years from June 2014 to June 2017. All the moorings had similar instrument configurations and were equipped with acoustic Doppler current profiles (ADCPs), recording current meters (RCMs), and T/S chains (consisting of CTDs and temperature loggers with a vertical resolution of 10 or 20 m in the upper 450 m and 50 m below 450 m). A schematic diagram of the mooring configurations can be found in Fig. 1b. The actual configurations for the moorings slightly differed at different locations and in different years. The instruments generally functioned well except for several ones. For example, the upward-looking ADCP data at NS2 and EW3 in the first year and the temperature data at

EW1 in the third year were missing due to instrument malfunction. Moreover, the *T/S* chain data at NS4 in the third year were lost due to the break of cables. The detailed instrument information of all the moorings can be found in Tables S1–S3 in the online supplemental material.

The data processing is similar to our previous mooring-based studies (e.g., Zhang et al. 2015). Summarized briefly, all the original data were first hourly averaged and then linearly interpolated onto a 5 m interval in vertical. After that, a 2.5-day fourth-order Butterworth low-pass filtering was applied to remove the tidal and inertial signals. Finally, all the data were daily averaged. The daily subinertial velocity and temperature/salinity data were used for analysis in this study.

b. Satellite and reanalysis data

To depict the sea surface characteristics of KLC, the sea surface height (SSH) and sea level anomaly (SLA) data distributed by the Copernicus Marine Environment Monitoring Service (CMEMS) were used in this study. The data product has merged different altimeter missions: *Jason-3*, *Sentinel-3A*, *HY-2A*, *SARAL*, *Cryosat-2*, *Jason-2*, *Jason-1*, TOPEX/Poseidon, *Envisat*, *GFO*, and *ERS-1/-2*. The temporal and spatial resolutions of the product are one day and 1/4°, respectively. The daily SSH and SLA data from 1993 to 2019 were downloaded and used here. In addition to the altimeter data, the near-surface concentration of chlorophyll-a (CHL-a) of the Moderate Resolution Imaging Spectro-radiometer (MODIS) data was also used in this study to examine the KLC characteristics in winter of 2016/17. The CHL-a product has a temporal resolution of 8 days and a spatial resolution of 4 km.

To further investigate the interannual modulation mechanism of the KLC, the 10 m reanalysis wind data between 1993 and 2019 from the European Center for Medium-Range Weather Forecasts (ECMWF) and the Hybrid Coordinate Ocean Model (HYCOM) reanalysis product between June 2016 and June 2017 were also used in this study. Both the ECMWF and HYCOM data have daily temporal resolution and their horizontal resolutions are 1/4° and 1/12°, respectively. Vertically, the HYCOM reanalysis product has 33 levels with a resolution of 10 m near the surface and 500 m near the bottom of 5500 m. Validations of the HYCOM data in the NESCS have been conducted previously by Zhang et al. (2013) and Park and Farmer (2013) through comparison with long-term in situ observations.

c. Identification of the KLC events

To investigate the interannual variability of the KLC, we first identified the strong KLC events from the historical altimeter data between 1993 and 2019. Here, a KLC event is defined when it meets the first two following criteria and a strong KLC event is defined when the third criterion is further satisfied: 1) the Kuroshio axis extends west of 119°E and presents a loop structure in the NESCS with its northern branch bending clockwise back to the Pacific; 2) the relative vorticity southwest of Taiwan (averaged over 20°–22.5°N, 118°–120.5°E, red box in Fig. 2h) should exceed two standard deviations relative to the time-mean value (Fig. 2j, red dashed line; i.e., $-1 \times 10^{-5}\,\mathrm{s}^{-1}$); 3) the lifespan of KLC should be longer than 50 days. Here, the axis of KLC is defined as the SSH contour that originates from east of the Luzon Island (west of 124°E) and has the maximum surface meridional velocity therein. Definition of the KLC's lifespan is the same with that in Zhang et al. (2017). Based on the first two criteria, 21 KLC events were identified, which is generally consistent with the 19 KLC eddy shedding events in Zhang et al. (2017) between October 1992 and October 2014. When the third criterion was applied, nine strong KLC events were screened out (Figs. 2a–i). The detailed information of these nine strong KLC events can be found in Table 1.

3. General observed results between 2014 and 2017

In this section, general characteristics of the KLC were depicted based on the concurrent moored and satellite data between 2014 and 2017. Figure 3 presents the depth–time plots of the zonal velocity above 800 m from six moorings (NS1–NS3, EW2–EW4). It can be seen that the direction of zonal velocity at site NS1 was opposite to the other sites, especially in winter. Specifically, the zonal velocity at NS1 was dominantly eastward, while at the other sites it was primarily westward. The maximum eastward and westward velocity occurred at NS1 and EW2 in January 2017, respectively, with their respective velocity reaching 0.93 and $-1.44\,\mathrm{m\,s}^{-1}$. During that time, the westward velocity at NS3 also reached $-1.13\,\mathrm{m\,s}^{-1}$. With respect to the meridional velocity, for most of the time in the three years, all the moorings showed strong positive values corresponding to the northward-flowing Kuroshio (Fig. S1). However, during the strong KLC event in 2016/17 winter, large southward velocities were also observed at the moorings NS1–NS3 and EW2–EW4.

In Fig. 4, we show the monthly distributions of altimeter SSHs and geostrophic currents and mooring-observed zonal velocity along the NS section. From the altimeter observations in Fig. 4a, it can be clearly seen that the Kuroshio strongly intruded into the SCS in a loop path in winter (the winter refers to November–February hereafter), while in summer, the Kuroshio was mainly in the leap state. In winter, the southern and
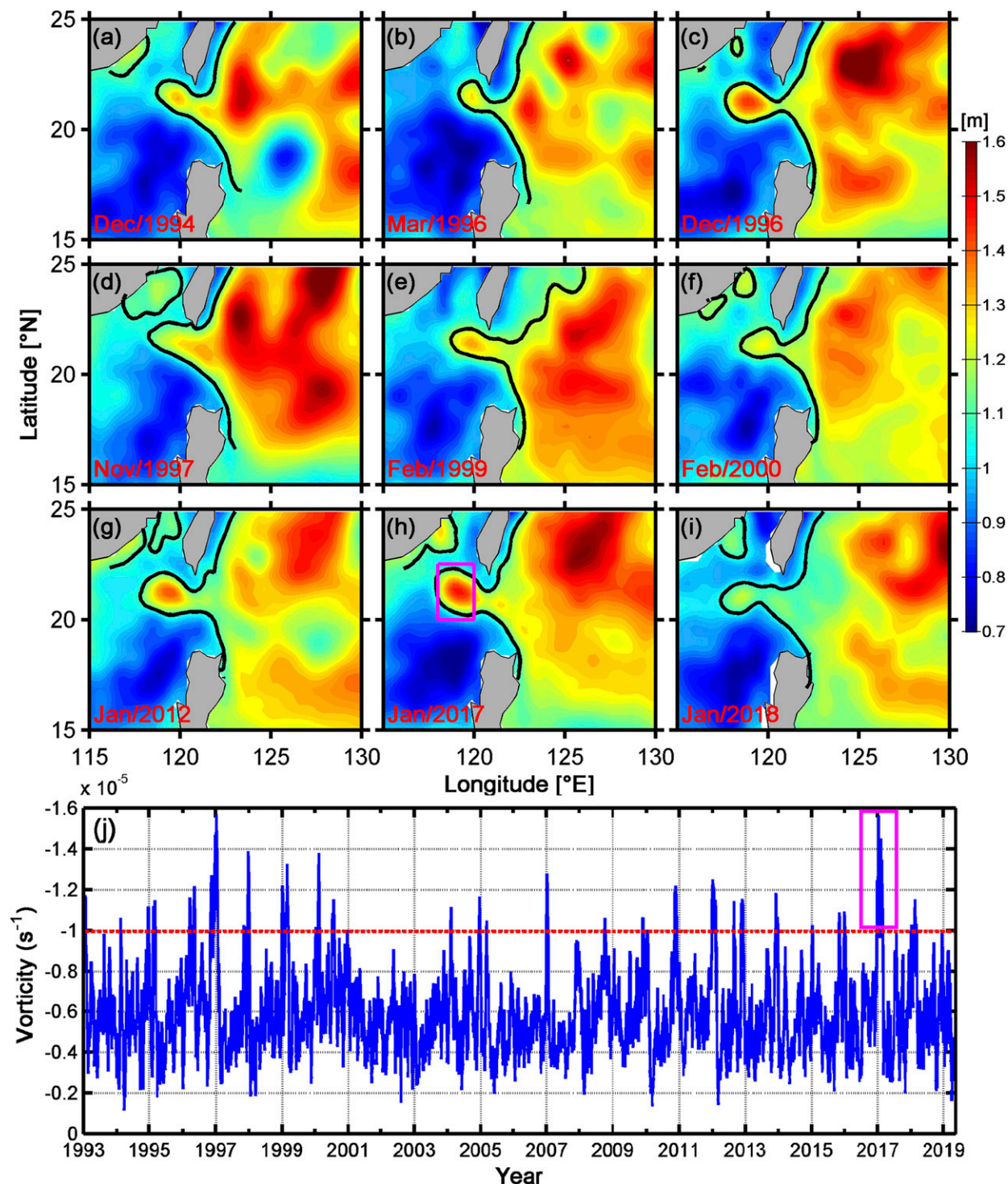
FIG. 2. (a)–(i) Distributions of the monthly mean SSH of the nine strong KLC events between 1993 and 2019. Black solid lines indicate the KLC axes. Note that in these figures, the SSH trend of 0.32 cm yr^{-1} due to the global warming has been removed from the original SSH. The month and year are marked on the bottom-left corner of each subplot. (j) Time series of the area-averaged negative relative vorticity in the KLC region [purple box in (h) 20°–22.5°N, 118°–120.5°E]. Red dashed line denotes the mean vorticity minus twice of its standard deviation. The strong KLC event in 2016/17 winter is marked using pink square in (h) and (j).

TABLE 1. Information of the nine strong KLC events between 1993 and 2019. Note that the SSH trend of 0.32 cm yr^{-1} that was calculated using the altimeter SSH data in the NESCS has been removed from the original SSH data.

No.	Start data of KLC	End data of KLC	Lifespan of KLC (days)	Maximum vorticity (10^{-5} s^{-1})	Maximum SSH (m)	Maximum SLA (m)	Shedding eddy or not?
1	2 Nov 1994	14 Feb 1995	105	−1.15	1.39	0.31	Yes
2	23 Dec 1995	6 Mar 1996	75	−1.21	1.37	0.30	No
3	16 Oct 1996	10 Jan 1997	87	−1.57	1.50	0.46	Yes
4	21 Oct 1997	22 Dec 1997	63	−1.39	1.33	0.27	Yes
5	17 Dec 1998	27 Feb 1999	73	−1.32	1.42	0.36	No
6	24 Nov 1999	8 Feb 2000	77	−1.38	1.41	0.41	Yes
7	21 Nov 2011	14 Jan 2012	55	−1.25	1.51	0.51	Yes
8	19 Oct 2016	8 Feb 2017	113	−1.57	1.56	0.62	Yes
9	21 Dec 2017	25 Feb 2018	67	−1.15	1.29	0.33	Yes

northern branches of the KLC were around sites NS3 and NS1, respectively. The westward extension of the KLC axis reached as far as 117.5°E. In the other seasons, the Kuroshio kept in a leap state that directly reached east of Taiwan without a branch into the SCS. Corresponding to the altimeter results, the mooring-observed zonal velocity at the NS section also presented an anticyclonic pattern in winter with westward and eastward velocities in the south and north, respectively (Fig. 4b). The strongest

zonal velocity occurred in January when the maximum westward velocity exceeded −0.53 m s^{-1} and the −0.1 m s^{-1} isoline extended down to the 350 m depth.

In addition to the distinct seasonal variability, the KLC also varied year to year (Fig. 5). During the 3-yr observation period, the strength of KLC was moderate in 2014/15 winter, weakest in 2015/16 winter, and strongest in 2016/17 winter. From the distributions of SSHs and geostrophic currents in winters of 2014–17,
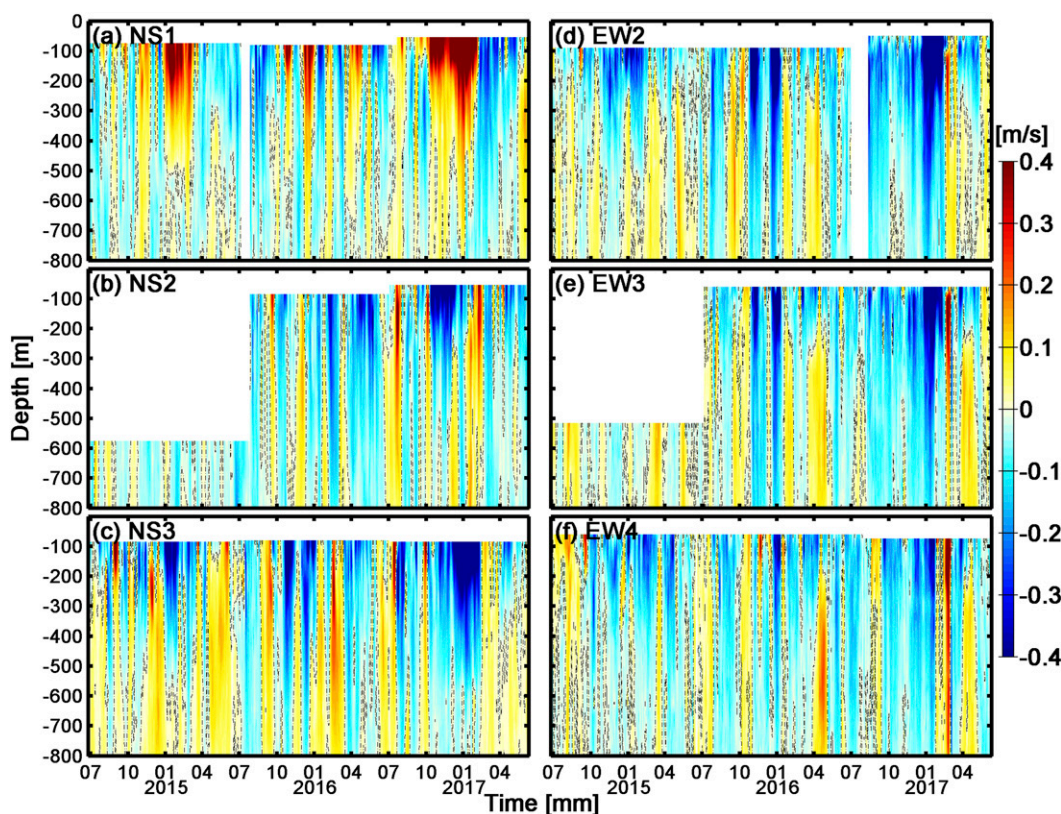

FIG. 3. Depth–time distributions of the daily averaged subinertial zonal velocity from June 2014 to June 2017 at sites (a)–(c) NS1–NS3 and (d)–(f) EW2–EW4, respectively. The black dashed line indicates the zero-velocity contour.
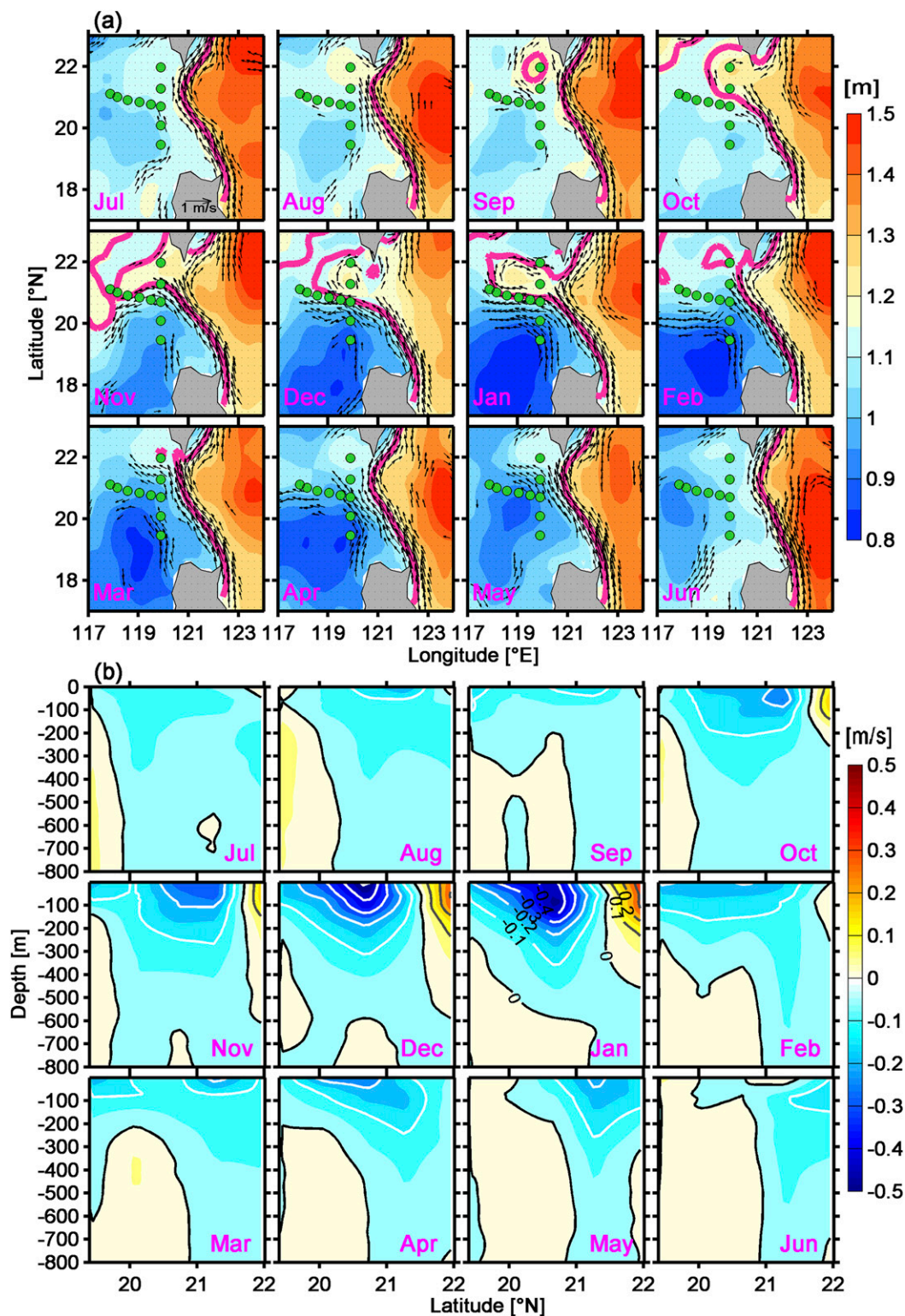
FIG. 4. (a) The monthly composite SSHs (shadings) and surface geostrophic currents (arrows) in the NESCS and the northwestern Pacific during the observation period. Here, only the velocities with magnitudes larger than $0.25 \, \mathrm{m \, s^{-1}}$ are shown. The green circles denote locations of the moorings. The purple thick lines represent axes of the Kuroshio. (b) The monthly composite zonal velocity across the NS section. White (gray) lines indicate the contours of westward (eastward) velocities with an interval of $0.1 \, \mathrm{m \, s^{-1}}$. Black line indicates the zero velocity contour. The months are marked in the bottom-left or bottom-right corner of each subplot.
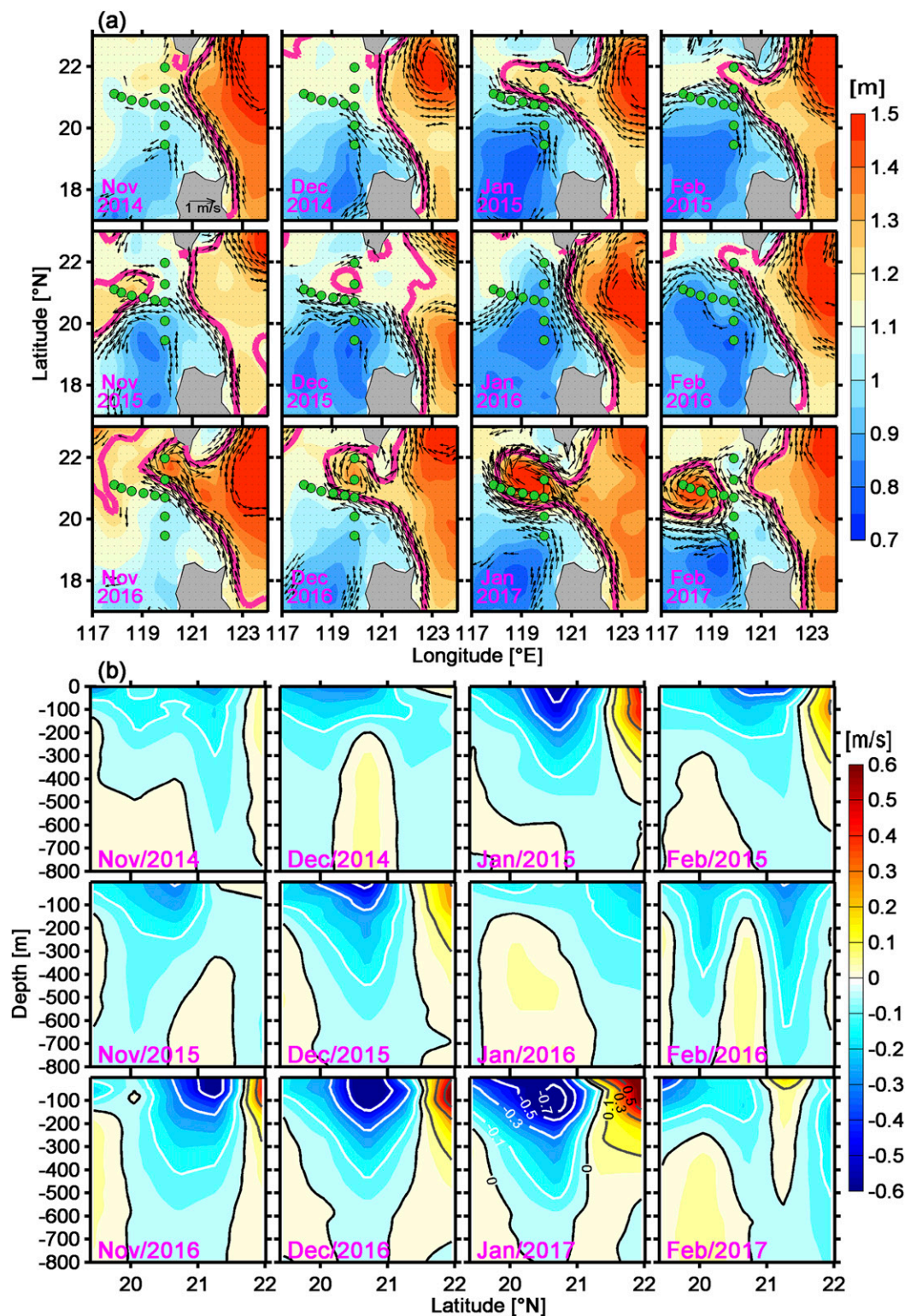
FIG. 5. As in Fig. 4, but it shows the mean result in each month of the three winters. The month and year are marked on the bottom-left corner of each subplot. Note that the contour interval in (b) is $0.2\,\mathrm{m\,s^{-1}}$, twice of that in Fig. 4b.

we can infer that the loop structure lasted for about 2, 1, and 4 months in the three winters, respectively. The maximum monthly mean SLA associated with the three KLCs were 19, 13, and 49 cm, respectively. The mooring-observed zonal velocity at the NS section presented characteristics similar to the altimeter results. The maximum monthly mean westward (eastward) zonal velocity during the three winters was -0.58 (0.54), -0.57 (0.31), and -0.83 (0.77) m s^{-1}, respectively. All the above results demonstrated that the KLC had a strong interannual variability during the observation period.

Through examining water mass properties, it is found that the water within the KLC in the upper layer (above $\sim$320 m) showed similar T/S characteristics with the Pacific Kuroshio water (Fig. S2). The salinity maximum of the KLC water even exceeded 34.94 psu, much larger than the NESCS local water (maximum salinity of 34.62 psu). In addition, CHL-a within and surrounding the KLC was much lower than that in the NESCS due to the fact that the Kuroshio water is more nutrient oligotrophic than the NESCS upper ocean (Fig. S3). These results demonstrated that the KLC can indeed transport a huge amount of warm, salty, and nutrient oligotrophic Pacific water into the SCS that will greatly influence the heat, salt, and nutrient balance of the SCS and therefore strongly modulate the biogeochemical processes (Xiu et al. 2016; Zhang et al. 2017).

4. Three-dimensional structure of the KLC

Using the method described in section 2, a total of nine strong KLC events were finally identified based on the historical altimeter data between 1993 and 2019. By comparing these nine strong KLC events, we found that the KLC event in 2016/17 winter is the strongest one since 1993 in respect to the SLA (62 cm), relative vorticity (-1.57×10^{-5} s^{-1}) and lifespan (113 days) (Fig. 2, Table 1). Given the strong strength and long lifespan of the KLC in 2016/17 winter, observational results from our mooring array provided us a unique opportunity to investigate its full-depth 3D structure as well as its evolution processes.

In Fig. 6, we show the detailed evolution progresses of this strong KLC event based on the altimeter observations. This KLC event started from 19 October 2016 when a loop-shaped flow structure began to form southwest of Taiwan. At that time, both the central SLA and the size of KLC were small (SLA $\sim$27 cm, horizontal scale $\sim$100 km). Then, the KLC rapidly grew and extended toward southwest until it became strongest on 6 February 2017. At this stage, the maximum SLA of the KLC exceeded 62 cm and its zonal and meridional scales reached $\sim$300 and $\sim$250 km, respectively. On 9 February

2017, an AE was shed from the KLC (i.e., detached from the Kuroshio axis), which indicated the end of the KLC event. Interestingly, a cyclonic eddy (CE) was generated behind the shedded AE, which is consistent with the conclusion of Zhang et al. (2017) that the trailing CE facilitates the shedding of AE from the KLC. After its generation, the AE gradually propagated southwestward and eventually disappeared in June 2017 near the Zhongsha Islands (figure not shown).

In Fig. 7, we show the depth–time plots of the temperature and temperature anomaly (T') at sites NS2, EW2, and EW4 during the strong KLC event in 2016/17 winter. Here, T' was obtained by subtracting the mean temperature in August–September 2016 and April–May 2017 at each mooring when no KLC and mesoscale eddies were present. It is found that, corresponding to the anticyclonic KLC and its shedded eddy, the thermocline at all three sites was deepened, resulting in positive T' from near surface to at least the 800 m depth. At the mooring sites NS2, EW2, and EW4 from east to west, the maximum thermocline displacement (here approximately represented by the displacement of the 16°C isotherm) and the maximum T' were (130, 170, 230 m) and (6.8°, 8.4°, 9.4°C), respectively; the dates of the maximum thermocline variation were on 13 January, 3 February, and 15 February 2017, respectively. These results suggested that the center of the KLC gradually migrated from east to west between December 2016 and February 2017 and its strength increased during the westward migration process. It should be noted that the time length of the thermocline depression at EW4 (only 1 month) was much shorter than the other two sites. This is because the site EW4 was actually influenced by the shedded AE, which migrated westward much faster than the KLC itself. The 230 m thermocline displacement and 9.4°C T' caused by the shedded AE observed here were much larger than the 120 m and 7.5°C of the AE reported by Zhang et al. (2013) in the same region in 2011/12 winter.

Given that the KLC was at the mature stage in January 2017 (prior to the eddy shedding), we depicted here its mean 3D structure in this month by combining the altimeter and moored data. From the mean SSHs and surface geostrophic currents in Fig. 8a, we found that the KLC presented an evident semienclosed and anticyclonic loop structure that influenced most of the moorings in January. This anticyclonic loop structure can also be clearly seen from the subsurface current velocities above 500 m with the southwestward, northwestward, and southeastward velocities at moorings NS3–NS4, EW1–EW5, and NS1–NS2, respectively (Figs. 8b–f). Below 500 m, the northern branch of the loop structure (with eastward zonal velocity) became obscure, although
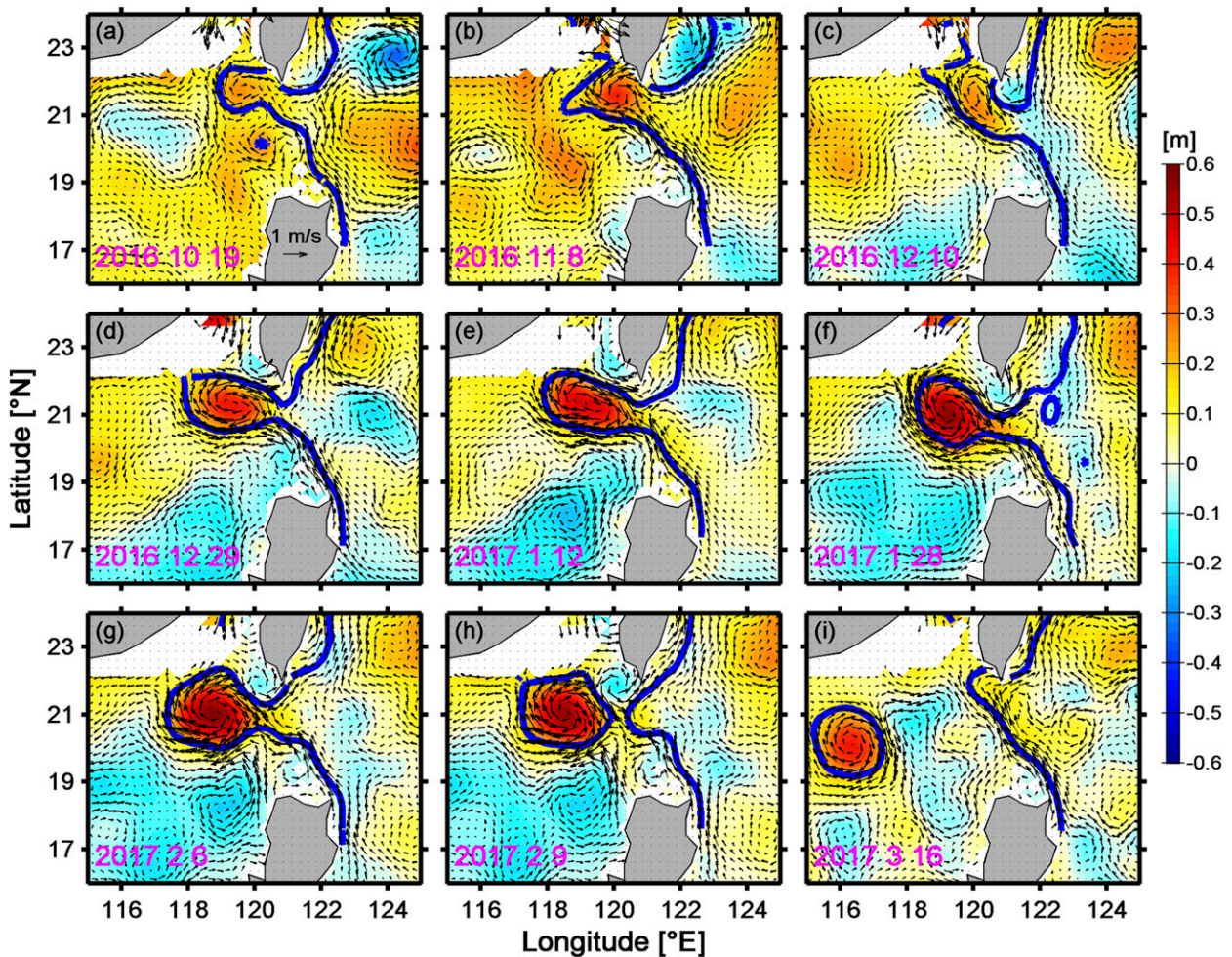
FIG. 6. Evolution processes of the strong KLC event in 2016/17 winter. Shading and arrows represent the altimeter SLA and geostrophic currents, respectively. The blue thick lines denote axes of the KLC and its shedding eddy. The date of each subplot is marked on the bottom-left corner.

the westward zonal velocity at mooring NS3 still persisted (Figs. 8g–i). This result suggested that the KLC was largely confined to the upper 500 m near the Luzon Strait, which generally agreed with the penetration depth of the upstream Kuroshio Current (Lien et al. 2014, 2015) and the water mass characteristics shown in Fig. S2. Based on the water mass anomaly method proposed by Zhang et al. (2017), we estimated that the volume of Kuroshio water trapped within the KLC in 2016/17 winter was $1.66 \times 10^{13} \, \mathrm{m}^3$, accounting for 12% of the integrated water volume across the NS section during the KLC period ($1.37 \times 10^{14} \, \mathrm{m}^3$, between 19 October 2016 and 8 February 2017).

In contrast to the moorings NS1–NS2, the northwestward velocity at the moorings EW1–EW5 penetrated much deeper (i.e., from surface down to 2000 m) and its magnitude still reached $10 \, \mathrm{cm \, s}^{-1}$ at 800 m (Figs. 8i,k). To further clarify the dynamics of this phenomenon, we

calculated the kinetic energy conversion term (KC) between the barotropic and baroclinic flows based on the observation data at the EW section using the formula: $\mathrm{KC} = -\int [\overline{u'^2}(\partial \overline{u}/\partial x) + \overline{u'v'}(\partial \overline{v}/\partial x) + \overline{v'^2}(\partial \overline{v}/\partial y) + \overline{u'v'}(\partial \overline{u}/\partial y)] \, dz$. Derivation of the formula is similar to the time perturbation kinetic energy equation (Qiao and Weisberg 1998), except that $\overline{\mathbf{u}}$ denotes the depth-averaged barotropic velocity (0–2000 m) and $\mathbf{u}'$ denotes the baroclinic velocity obtained by subtracting $\overline{\mathbf{u}}$ from the original velocity. Positive (negative) KC means that baroclinic (barotropic) flow gains energy from the barotropic (baroclinic) flow (Scott and Wang 2005; Vallis 2006). Based on the evaluation using the moored data and HYCOM outputs, we found that the KC is dominated by the first two terms in the above formula (Fig. S4). Therefore, only the first two terms of the KC was calculated and shown here (based on moored data of the EW section). The calculated KC along the EW
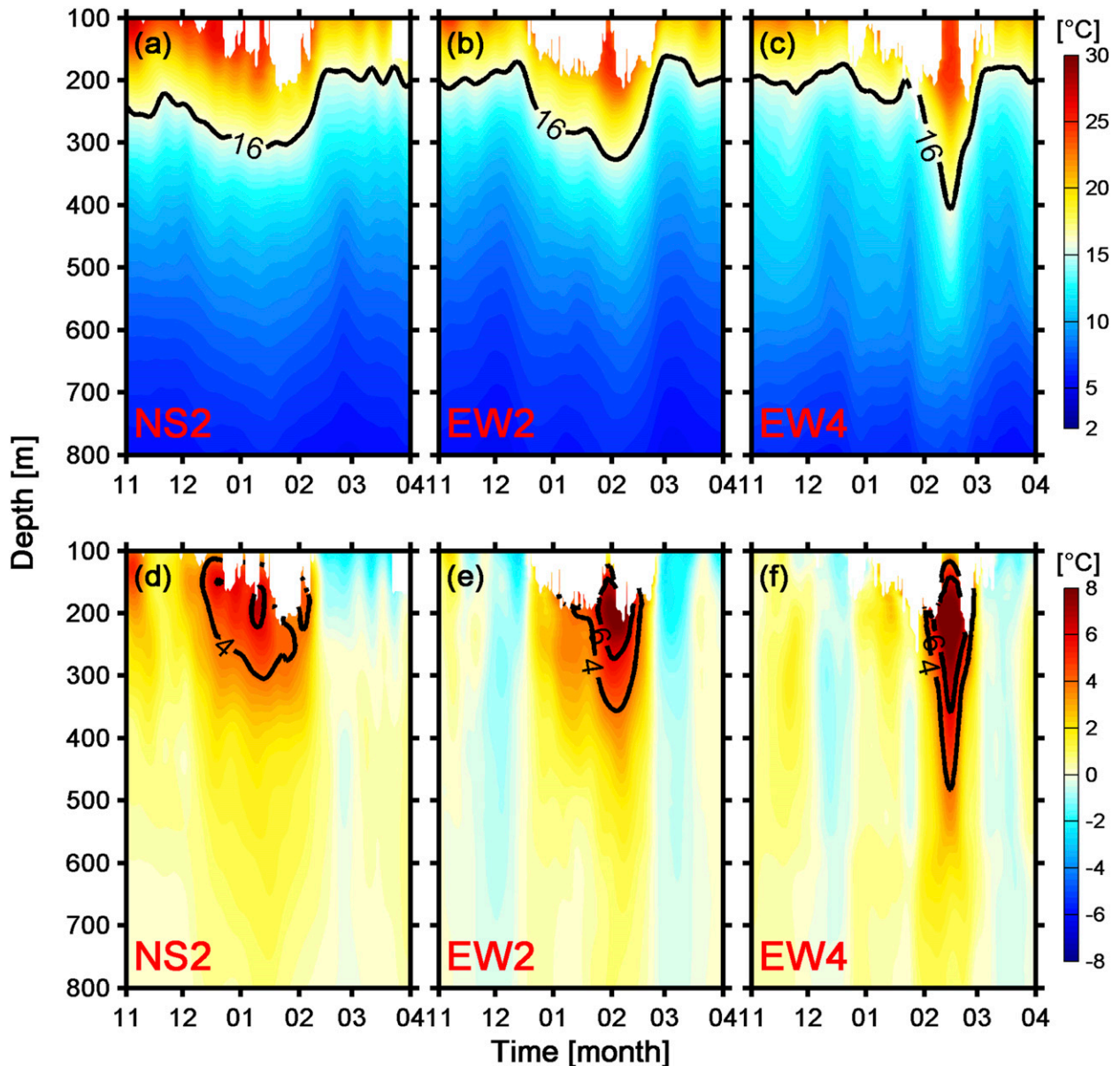
FIG. 7. (a)–(c) Depth–time plots of temperature at sites NS2, EW2, and EW4, respectively, from November 2016 to March 2017. Black lines denotes the 16°C isotherms. (d)–(f) As in (a)–(c), but for the temperature anomaly. The temperature anomalies were calculated on the Z levels. The 4° and 6°C temperature anomaly contours are indicated by black lines.

section showed significant negative values in late December 2016 and January 2017 (Fig. 9), indicating that the baroclinic flow transferred kinetic energy to the barotropic flow during the KLC's evolution. To our best knowledge, the above barotropization process of the KLC is reported here for the first time. This result also well explains why the AE shedded from the originally baroclinic KLC becomes a full-depth phenomenon in the SCS interior (Zhang et al. 2013, 2016). With respect to T' corresponding to the deepened thermocline induced by

the KLC, it showed positive values near the center of KLC (at moorings NS2–NS3 and EW2–EW4). In contrast, at the moorings near the periphery or outside of the KLC, T' was observed close to zero (Figs. 8b–i).

5. Interannual modulation mechanism of the KLC

The concurrent moored and satellite observations demonstrated that the KLC shows strong interannual variabilities. In this section, the interannual modulation
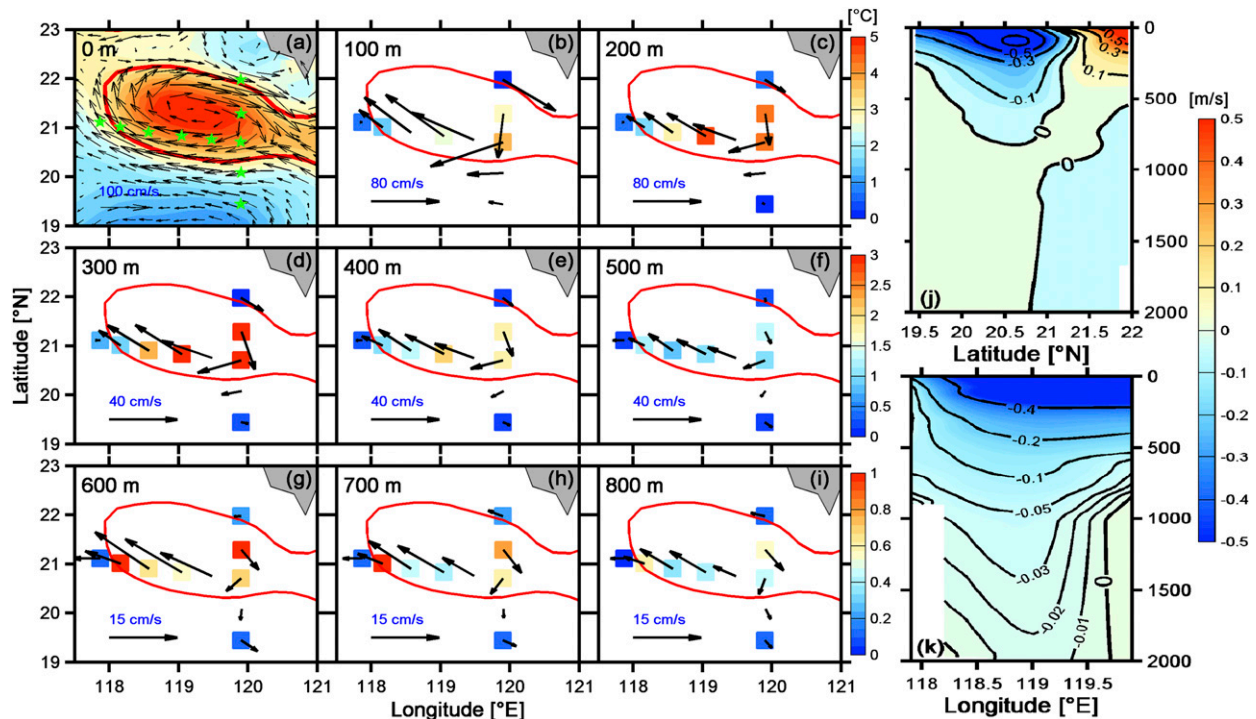
FIG. 8. Three-dimensional structure of the strong KLC averaged in January 2017 when the KLC was at the mature stage. (a) Distributions of the altimeter SSHs (shading) and surface geostrophic currents (arrows). The red line indicates axis of the KLC in January 2017. Green stars represent the mooring locations. (b)–(i) Distributions of the mooring-observed temperature anomaly (shading) and velocity (black arrows) at depths from 100 to 800 m every 100 m. The depths are marked in the upper-right corner of each subplot. Note that the colorbars of temperature anomalies are different for (b) and (c), (d)–(f), and (g)–(i). (j),(k) Vertical distributions of the zonal velocity at the NS section and EW section, respectively. Black lines indicate velocity contours.

mechanism of the KLC will be discussed by combining dynamical energetics analysis and statistical composite analysis.

a. Energetics analysis of the KLC in 2016/17 winter

The concurrent moored and satellite observations between 2014 and 2017 suggested that the KLC was moderate, weakest, and strongest in the winters of 2014/15, 2015/16, and 2016/17, respectively (recall section 3). By examining the northeast monsoon wind in the SCS, it is found that its strength showed a similar interannual variation with the KLC during these three winters (Figs. 10a–c). The strengthened (weakened) northeast monsoon in the 2016/17 (2015/16) winter was closely associated with the prevailing La Niña (El Niño) event at that time when the surface wind field was dominated by an anomalous cyclone (anticyclone) over the northwestern Pacific (Wang et al. 2000; Zhao and Zhu 2016). Corresponding to the anomalous monsoon wind, the wind stress curl (WSC) anomaly in the 2016/17 (2015/16) winter showed strong negative (positive) values southwest of Taiwan (Figs. 10a–c), which can induce negative (positive) relative vorticity anomaly in the ocean (Figs. 10d–f;

Wang et al. 2008) and provide a favorable (unfavorable) condition for the development of an anticyclonic KLC.

To quantify the role of wind in the interannual variation of KLC, the energetics analysis was carried out
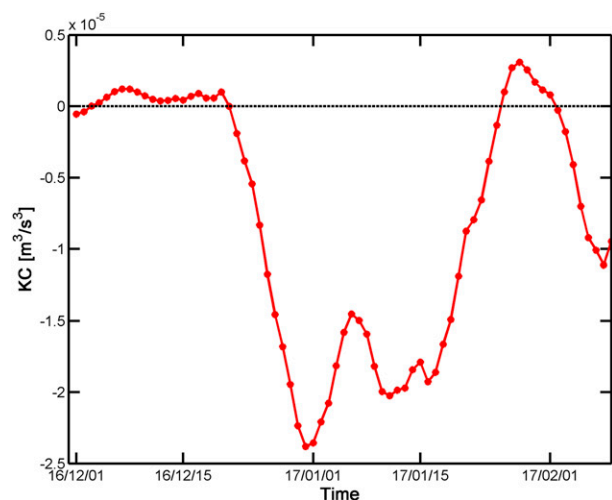

FIG. 9. Time series of the KC term averaged in the upper 2000 m, calculated based on the moored data at section EW.
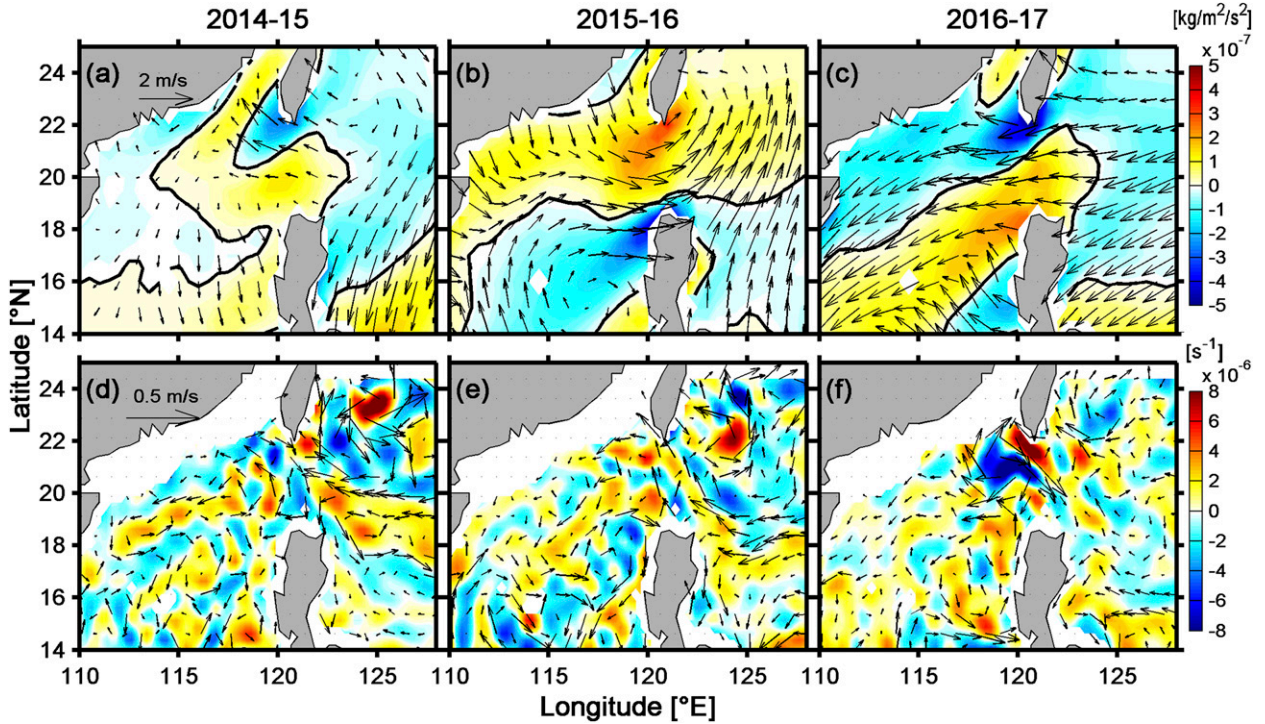
FIG. 10. (a)–(c) Distributions of anomalous wind velocity (arrows) and WSC (shading) in the winters of 2014/15, 2015/16, and 2016/17, respectively. The anomalies were obtained by subtracting climatologically winter mean values between 1993 and 2019. The black line denotes the zero WSC anomaly contour. (d)–(f) As in (a)–(c), but for the anomalous surface geostrophic velocity (arrows) and relative vorticity (shading) derived from altimeter data.

during the strong KLC event in 2016/17 winter. Specifically, the rate of wind stress work input into the KLC was integrated from the beginning to the end date of the KLC (from 19 October 2016 to 8 February 2017) and the calculated wind work (WW) was then compared with the increased mechanical energy (ME, including kinetic energy and available potential energy) of the KLC during this period. The ME and WW were calculated using the following Eq. (1) and Eqs. (2) and (3), respectively:

$$\text{ME} = \frac{1}{m}\sum_{i=1}^{m}\int_{-1000}^{0}\left[\frac{1}{2}\rho_0(\overline{\mathbf{v}\cdot\mathbf{v}}) + \frac{g^2}{2N^2}\overline{\frac{\rho'^2}{\rho_0}}\right]dzS, \quad (1)$$

$$\text{WW} = \iiint\overline{\boldsymbol{\tau}_w\cdot\mathbf{v}_0}\,dx\,dy\,dt, \quad (2)$$

$$\boldsymbol{\tau}_w = \rho_a C_{ds}|\mathbf{v}_w - \mathbf{v}_0|(\mathbf{v}_w - \mathbf{v}_0), \quad (3)$$

In the above equations, the overbar denotes a 30-day running mean, the prime denotes anomalies from the 3-yr time mean at every mooring location, $\mathbf{v}$ is the current velocity, g is the gravity acceleration, N is the buoyancy frequency, and S and m are the area of the fixed box that fully contained the KLC (19.5°–22.7°N, 117.5°–120.7°E;

red box in Fig. 11c) and the number of moorings within the KLC region ($m = 9$, NS1–NS4, EW1–EW5), respectively. Parameters $\mathbf{v}_0$, $\boldsymbol{\tau}_w$, and $\mathbf{v}_w$ are the surface geostrophic current of satellite data, wind stress, and wind velocity from the ECMWF data, respectively. Parameter C_{ds} is a drag coefficient as a function of wind speed (Large and Pond 1981). Parameter $\rho_0 = 1030\,\text{kg m}^{-3}$ and $\rho_a = 1.2\,\text{kg m}^{-3}$ are the mean seawater and air density, respectively. In each day, ME of the KLC was estimated based on the moored data, and the vertical integral was from 1000 m to the sea surface.

From the time series of ME (Fig. 11e), we can see that it had increased $2.09 \pm 0.23 \times 10^{16}$ J from the beginning to the end date ($2.4 \pm 0.08 \times 10^{15}$ to $2.33 \pm 0.36 \times 10^{16}$ J). Given that the horizontal advection of ME across the fixed box cannot be estimated based on the moored data, its relative contribution was evaluated based on the HYCOM reanalysis data. We found that in the HYCOM-based results, the horizontal advection term was one order of magnitude smaller than the time change rate of ME. Therefore, the advection term was not considered in the mooring-based energetics analysis. Because both the velocity of KLC and the wind stress in the south were larger than those in the north,
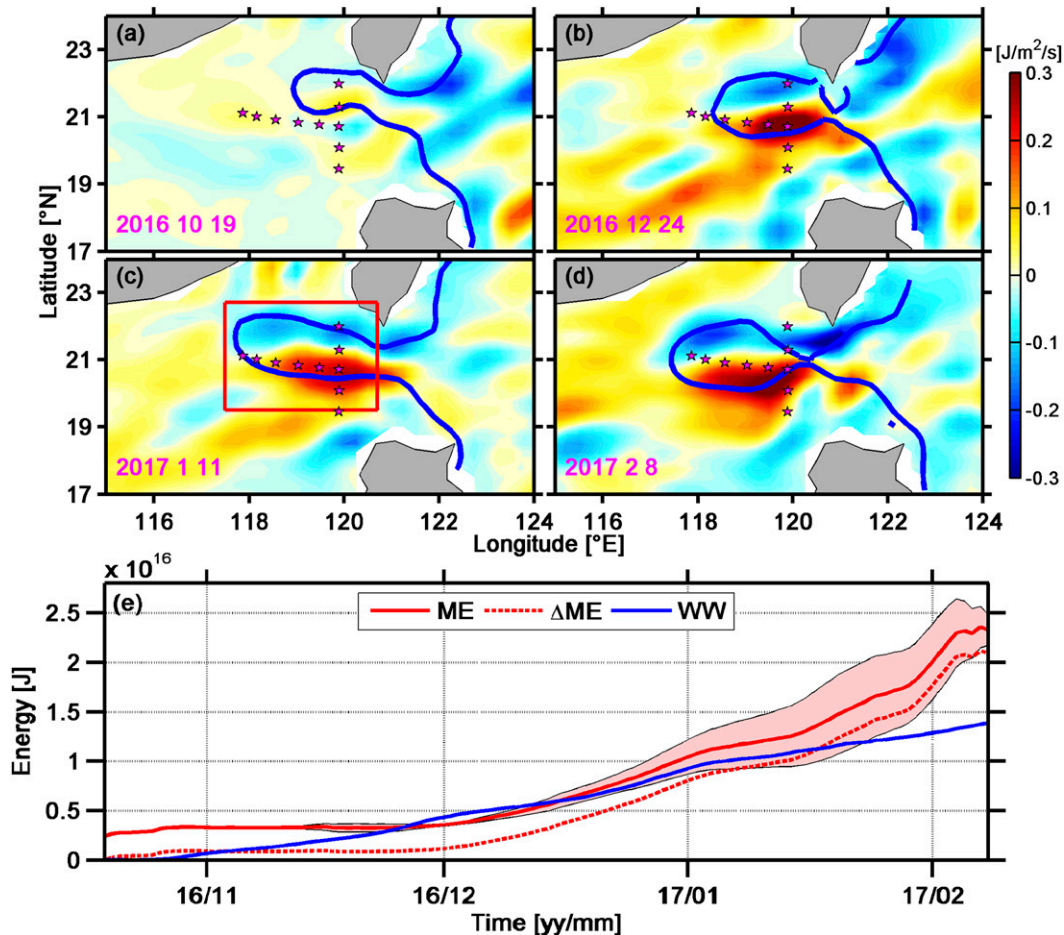
FIG. 11. (a)–(d) Distributions of wind stress work at different stages of the strong KLC. Blue lines indicate axes of the KLC. The red box in (c) denotes the region that fully contains the KLC (19.5°–22.7°N, 117.5°–120.7°E). Purple stars represent locations of the moorings. The date of each subplot is marked on the bottom-left corner. (e) Time series of the mechanical energy calculated based on the moored data (ME, red solid line), change of ME compared with the first day on 19 Oct 2016 (ΔME, red dashed line), and the wind stress work integrated from the first day on 19 Oct 2016 (WW, blue solid line) over the KLC region. The shading represents error bar of the ME, which is obtained from the HYCOM reanalysis data through comparing the area-mean ME with the point-mean ME at virtual mooring locations.

WW integrated in the KLC region was always positive (Figs. 11a–d). The time-integrated WW during this period was 1.38×10^{16} J (Fig. 11e). This result suggested that the WW could account for 66% of the increased energy of KLC if the dissipation processes were not considered. The above energetics analysis demonstrated that the strengthened monsoon wind associated with the La Niña event indeed played an important role in the development of this strong KLC event in 2016/17 winter.

b. Interannual modulation mechanism of the KLC between 1993 and 2019

The moored observations were only available between 2014 and 2017. To examine whether the mechanism revealed by the above energetics analysis is universal, the interannual variation of the KLC was further analyzed using the long-term altimeter and wind data between 1993 and 2019. Before the detailed analysis, we first defined the winter mean area-averaged surface negative relative vorticity in the KLC region (purple box in Fig. 2h) as an index to represent the strength of KLC (recall the KLC identification method in section 2). In Fig. 12a, we compare the KLC index with the mean absolute wind speed southwest of Taiwan (purple box in Fig. 2h) in all of the winters between 1993 and 2019. The result shows that the KLC was stronger in the winters of 1994/95, 1995/96, 1996/97, 1998/99, 1999/2000, 2000/01, 2007/08, 2010/11, 2011/12, 2016/17, and 2017/18 (11 stronger KLC events), and weaker in the winters of 1993/94, 1997/98, 2001/02, 2002/03, 2003/04, 2004/05,
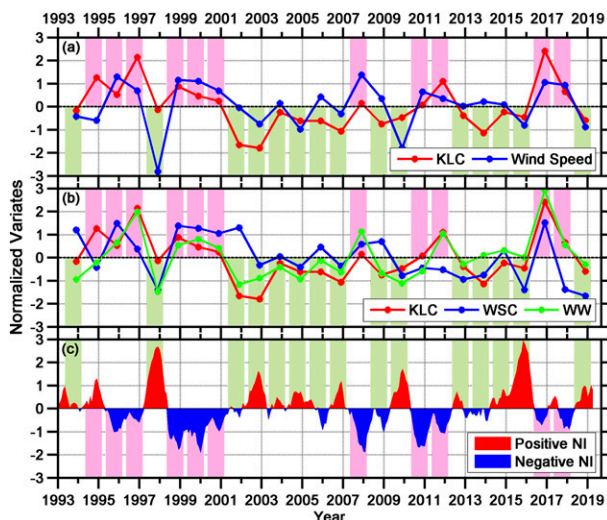
FIG. 12. (a) Time series of the KLC index (red line) and wind speed (blue line) averaged in the KLC region (i.e., the box in Fig. 2h). All the time series have been normalized by removing the mean and then being divided by the standard deviation. (b) As in (a), but the blue and green lines denote strength of WSC and WW averaged in the KLC region, respectively. (c) Time series of Niño-3.4 index with positive and negative values indicated by red and blue colors, respectively. In all the three subplots, pink and green shading represent stronger-KLC and weaker-KLC events, respectively.

2005/06, 2006/07, 2008/09, 2009/10, 2012/13, 2013/14, 2014/15, 2015/16, and 2018/19 (15 weaker KLC events, including the winters without KLC). For the 11 stronger (15 weaker) KLC events, 91% (67%) of them corresponded to stronger (weaker) wind speed compared with the climatological state. Comparisons with the WW and WSC showed similar results (Fig. 12b). Specifically, during 82% (73%) of the 11 stronger KLC events, the WW (WSC) was stronger than the mean state, while during 87% (67%) of the 15 weaker KLC events, the WW (WSC) was weaker than the mean state. Furthermore, the KLC index was found to be closely correlated with the Niño-3.4 index, i.e., 10 of the 11 stronger KLC events occurred in La Niña years, while 11 of the 15 weaker KLC events occurred in El Niño years (Fig. 12c). The composite distributions of SSH, surface geostrophic velocity, wind anomaly, WSC anomaly and WW in Fig. 13 (see also Fig. S5) further suggested that during La Niña years, the winter northeast monsoon, the negative WSC and the positive WW southwest of Taiwan are strengthened and, correspondingly, the KLC structure becomes stronger; the situation is reversed during El Niño years. Overall, the above statistical results demonstrated the role of ENSO in modulating the KLC strength through changing the winter wind field over the NESCS, which further confirms our conclusion drawn based on the 3-yr moored data (i.e., the previous subsection).

As argued by many previous studies, Pacific meso-scale eddies (e.g., Chang et al. 2015; Zhao et al. 2016; Zheng et al. 2019; Yang et al. 2020) and nonlinear hysteresis of the upstream Kuroshio east of the Luzon Island (e.g., Sheremet 2001; Yuan and Wang 2011) can also influence the formation and development of the KLC. Through examining the altimeter observations during the strong KLC event in 2016/17 winter, we indeed found that an AE in the northwestern Pacific perturbed the Kuroshio path in autumn and its front portion then penetrated across the Luzon Strait, which may have contributed to the formation of the nascent KLC in October (Fig. S6). However, by comparing the KLC index with the strength of AEs in autumn (August–November) east of the Luzon Strait (the integrated negative relative vorticity in the region of 19°–22°N, 121°–123°E was used to represent the strength of Pacific AEs), we did not find a significant correlation between them (Fig. 14a). In Fig. 14b, we also compared the KLC index with the upstream Kuroshio strength in autumn east of the Luzon Island. Here, the Kuroshio strength was calculated by integrating the surface meridional geostrophic current along the 18°N section between the Luzon Island and 124°E. Again, from the comparison, no significant correlation is found. These statistical analysis results implied that neither the Pacific eddies nor the upstream Kuroshio strength played a decisive role in the interannual modulation of the KLC.

6. Summary

Based on mooring-array observations between June 2014 and June 2017 and the long-term satellite data, 3D structure and interannual variability of the KLC in the NESCS were investigated in this study. The observations demonstrated that the KLC is a robust phenomenon in the NESCS, which displays a semienclosed anticyclonic structure with westward and eastward zonal velocity in the central and northern Luzon Strait, respectively. However, different from the Loop Current in the Gulf of Mexico, the KLC in the NESCS is not a permanent current and it primarily occurs in autumn and winter. In the vertical direction, the KLC structure is originally confined to the upper 500 m near the Luzon Strait. However, when the KLC extends into the NESCS interior, barotropization occurs and its southern branch with westward flow can reach as deep as 2000 m. To our best knowledge, this barotropization process of the KLC is identified for the first time and it can well explain the equivalent barotropic structure of the AEs shed from the KLC as found by our earlier studies (e.g., Zhang et al. 2016).

During the 3-yr observation period, the KLC showed strong interannual variability and its strength was moderate,
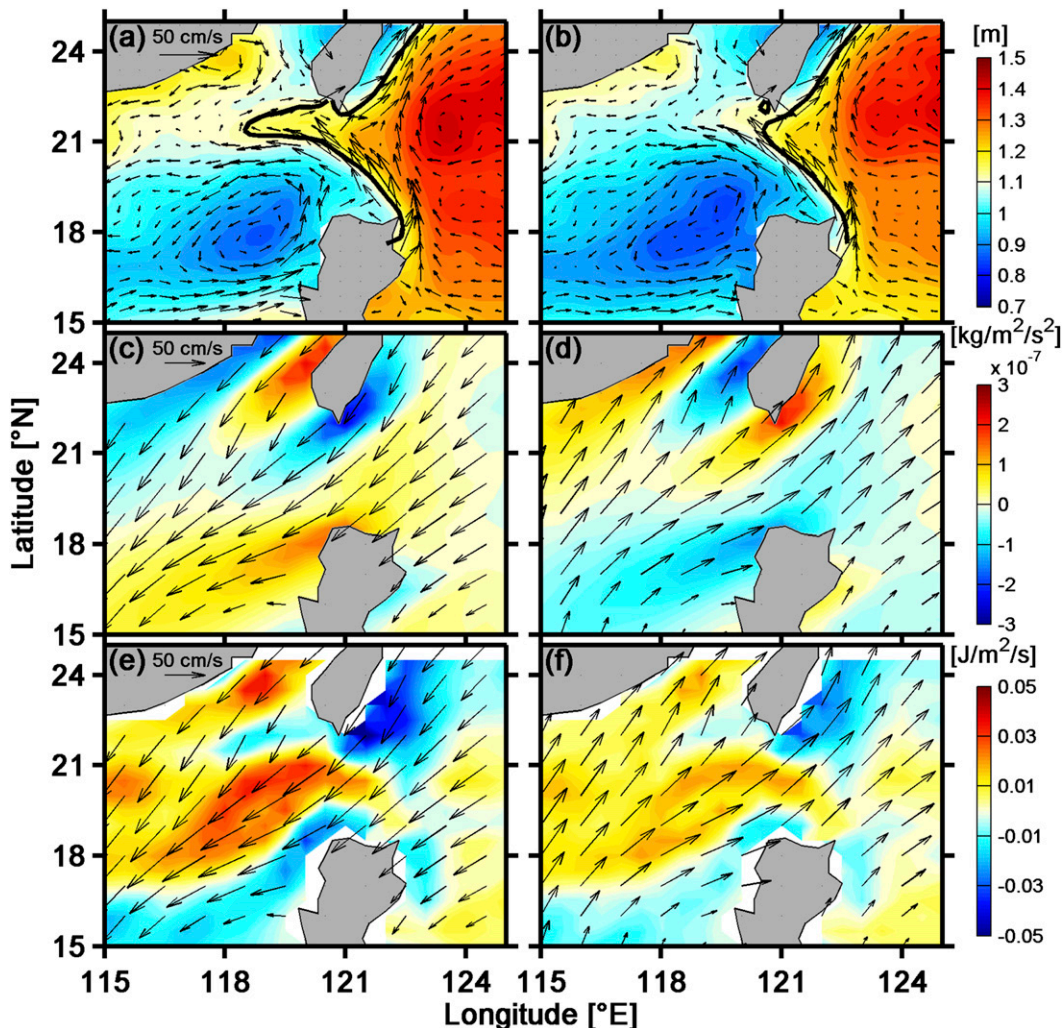
FIG. 13. (a),(b) Composite mean SSH (shading) and surface geostrophic current (arrows) distributions in the winters of La Niña and El Niño years, respectively. The black line denotes the Kuroshio axis. (c),(d) As in (a) and (b), but for the WSC anomaly (shading) and wind velocity anomaly (arrows) distributions. (e),(f) As in (c) and (d), but for the WW distributions.

weakest, and strongest in the winters of 2014/15, 2015/16, and 2016/17, respectively. Through examining the historical altimeter data between 1993 and 2019, it is found that the KLC in 2016/17 winter is the strongest one since 1993. Energetics analysis showed that the WW accounted for 66% of the total energy increase of this strong KLC event and therefore, it played a significant role in the KLC's development. Based on statistical analysis between 1993 and 2019, we found that the interannual variation of KLC is strongly modulated by the ENSO phases. Specifically, during La Niña years, an anomalous atmospheric cyclone occurs in the northwestern Pacific, which strengthens the winter northeast monsoon in the NESCS. The strengthened wind inputs more negative vorticity and energy to the southwest of Taiwan and provides a favorable condition for the

development of KLC. The situation is reversed during El Niño years. Further analysis suggested that the Pacific mesoscale eddies and the nonlinear hysteresis of the upstream Kuroshio played insignificant roles in the interannual modulation of KLC. In another word, we found that the ENSO's impact on the interannual variation of KLC is primarily through the atmospheric bridge (i.e., local wind) rather than the oceanic bridge (i.e., Pacific eddies and Kuroshio strength). Because the KLC and its eddy shedding can have a large impact on the deep-ocean dynamics in the SCS (Zhang et al. 2013; Alford et al. 2015), it may provide an important route to transfer the ENSO's impact into the deep SCS that can further modulate the deep-ocean processes, such as internal waves, mixing, topographic waves, and deep-ocean submesoscales. This is
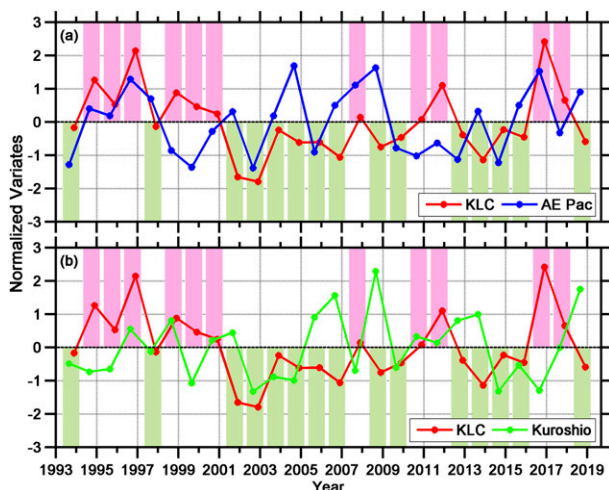
FIG. 14. (a) Time series of the KLC index (red line) and the strength of Pacific AEs (blue line). All the time series have been normalized by removing the mean and then being divided by the standard deviation. (b) As in (a), but the green dotted line denotes the strength of upstream Kuroshio.

an interesting topic that should be investigated in future studies.

REFERENCES

Alford, M. H., and Coauthors, 2015: The formation and fate of internal waves in the South China Sea. *Nature*, **521**, 65–69, https://doi.org/10.1038/nature14399.

Caruso, M. J., G. G. Gawarkiewicz, and R. C. Beardsley, 2006: Interannual variability of the Kuroshio intrusion in the South

China Sea. *J. Oceanogr.*, **62**, 559–575, https://doi.org/10.1007/ s10872-006-0076-0.

Centurioni, L. R., P. P. Niiler, and D.-K. Lee, 2004: Observations of inflow of Philippine Sea surface water into the South China Sea through the Luzon Strait. *J. Phys. Oceanogr.*, **34**, 113–121, https://doi.org/10.1175/1520-0485(2004)034<0113:OOIOPS> 2.0.CO;2.

Chang, Y. L., Y. Miyazawa, and X. Guo, 2015: Effects of the STCC eddies on the Kuroshio based on the 20-year JCOPE2 reanalysis results. *Prog. Oceanogr.*, **135**, 64–76, https://doi.org/ 10.1016/j.pocean.2015.04.006.

Farris, A., and M. Wimbush, 1996: Wind-induced Kuroshio intrusion into the South China Sea. *J. Oceanogr.*, **52**, 771–784, https://doi.org/10.1007/BF02239465.

Gan, J., Z. Liu, and C. Hui, 2016: A three-layer alternating spinning circulation in the South China Sea. *J. Phys. Oceanogr.*, **46**, 2309–2315, https://doi.org/10.1175/JPO-D-16-0044.1.

Guo, J., Y. Feng, Y. Yuan, and B. Guo, 2013: Kuroshio loop current intruding into the South China Sea and its shedding eddy. *Oceanol. Limnol. Sin.*, **23**, 675–689.

Ho, C.-R., Q. Zheng, N.-J. Kuo, C.-H. Tsai, and N. E. Huang, 2004: Observation of the Kuroshio intrusion region in the South China Sea from AVHRR data. *Int. J. Remote Sens.*, **25**, 4583–4591, https://doi.org/10.1080/0143116042000192376.

Hu, D., L. Wu, W. Cai, A. S. Gupta, and W. S. Kessler, 2015: Pacific western boundary currents and their roles in climate. *Nature*, **522**, 299–308, https://doi.org/10.1038/nature14504.

Huang, X., Z. Chen, W. Zhao, Z. Zhang, C. Zhou, Q. Yang, and J. Tian, 2016: An extreme internal solitary wave event observed in the northern South China Sea. *Sci. Rep.*, **6**, 30041, https://doi.org/10.1038/srep30041.

Jia, Y., and E. P. Chassignet, 2011: Seasonal variation of eddy shedding from the Kuroshio intrusion in the Luzon Strait. *J. Oceanogr.*, **67**, 601–611, https://doi.org/10.1007/s10872-011-0060-1.

Large, W. G., and S. Pond, 1981: Open-ocean momentum flux measurements in moderate to strong winds. *J. Phys. Oceanogr.*, **11**, 324–336, https://doi.org/10.1175/1520-0485(1981)011<0324: OOMFMI>2.0.CO;2.

Li, L., and Y. Wu, 1989: A Kuroshio loop current in the South China Sea? On circulation of the northeastern South China Sea (in Chinese with English abstract). *J. Oceanogr. Taiwan*, **8**, 89–95.

——, W. D. Nowlin, and S. Jilan, 1998: Anticyclonic rings from the Kuroshio in the South China Sea. *Deep-Sea Res. I*, **45**, 1469–1482, https://doi.org/10.1016/S0967-0637(98)00026-0.

Lien, R.-C., B. Ma, Y.-H. Cheng, C.-R. Ho, B. Qiu, C. M. Lee, and M.-H. Chang, 2014: Modulation of Kuroshio transport by mesoscale eddies at the Luzon Strait entrance. *J. Geophys. Res. Oceans*, **119**, 2129–2142, https://doi.org/ 10.1002/2013JC009548.

——, and Coauthors, 2015: The Kuroshio and Luzon undercurrent east of Luzon Island. *Oceanography*, **28**, 54–63, https://doi.org/ 10.5670/oceanog.2015.81.

Nan, F., H. Xue, F. Chai, L. Shi, M. Shi, and P. Guo, 2011: Identification of different types of Kuroshio intrusion into the South China Sea. *Ocean Dyn.*, **61**, 1291–1304, https://doi.org/ 10.1007/s10236-011-0426-3.

——, ——, and F. Yu, 2014: Kuroshio intrusion into the South China Sea: A review. *Prog. Oceanogr.*, **137**, 314–333, https:// doi.org/10.1016/J.POCEAN.2014.05.012.

Nitani, H., 1972: Beginning of the Kuroshio. *Kuroshio—Its Physical Aspects*, H. Stommel and K. Yashida, Eds., University of Tokyo Press, 129–163.

Park, J.-H., and D. Farmer, 2013: Effects of Kuroshio intrusions on nonlinear internal waves in the South China Sea during winter. *J. Geophys. Res. Oceans*, **118**, 7081–7094, https://doi.org/10.1002/2013JC008983.

Qiao, L., and R. H. Weisberg, 1998: Tropical instability wave energetics: Observations from the tropical instability wave experiment. *J. Phys. Oceanogr.*, **28**, 345–360, https://doi.org/10.1175/1520-0485(1998)028<0345:TIWEOF>2.0.CO;2.

Qiu, B., and R. Lukas, 1996: Seasonal and interannual variability of the North Equatorial Current, the Mindanao Current, and the Kuroshio along the Pacific western boundary. *J. Geophys. Res.*, **101**, 12 315–12 330, https://doi.org/10.1029/95JC03204.

Qu, T., Y. Y. Kim, M. Yaremchuk, T. Tozuka, A. Ishida, and T. Yamagata, 2004: Can Luzon Strait transport play a role in conveying the impact of ENSO to the South China Sea? *J. Climate*, **17**, 3644–3657, https://doi.org/10.1175/1520-0442(2004)017<3644:CLSTPA>2.0.CO;2.

Scott, R. B., and F. Wang, 2005: Direct evidence of an oceanic inverse kinetic energy cascade from satellite altimetry. *J. Phys. Oceanogr.*, **35**, 1650–1666, https://doi.org/10.1175/JPO2771.1.

Shaw, P., 1989: The intrusion of water masses into the sea southwest of Taiwan. *J. Geophys. Res.*, **94**, 18 213–18 226, https://doi.org/10.1029/JC094iC12p18213.

Sheremet, V. A., 2001: Hysteresis of a western boundary current leaping across a gap. *J. Phys. Oceanogr.*, **31**, 1247–1259, https://doi.org/10.1175/1520-0485(2001)031<1247:HOAWBC>2.0.CO;2.

Sheu, W. J., C. R. Wu, and L. Y. Oey, 2010: Blocking and westward passage of eddies in the Luzon Strait. *Deep-Sea Res. II*, **57**, 1783–1791, https://doi.org/10.1016/j.dsr2.2010.04.004.

Song, Y. T., 2006: Estimation of interbasin transport using ocean bottom pressure: Theory and model for Asian marginal seas. *J. Geophys. Res.*, **111**, C11S19, https://doi.org/10.1029/2005JC003189.

Sun, Z., Z. Zhang, W. Zhao, and J. Tian, 2016: Interannual modulation of eddy kinetic energy in the northeastern South China Sea as revealed by an eddy-resolving OGCM. *J. Geophys. Res. Oceans*, **121**, 3190–3201, https://doi.org/10.1002/2015JC011497.

Tian, J., Q. Yang, X. Liang, D. Hu, F. Wang, and T. Qu, 2006: Observation of Luzon Strait transport. *Geophys. Res. Lett.*, **33**, L19607, https://doi.org/10.1029/2006GL026272.

Vallis, G. K., 2006: *Atmospheric and Oceanic Fluid Dynamics: Fundamentals and Large-Scale Circulation.* Cambridge University Press, 745 pp.

Wang, B., R. Wu, and X. Fu, 2000: Pacific–East Asian teleconnection: How does ENSO affect East Asian climate? *J. Climate*, **13**, 1517–1536, https://doi.org/10.1175/1520-0442(2000)013<1517:PEATHD>2.0.CO;2.

Wang, G., D. Chen, and J. Su, 2008: Winter eddy genesis in the eastern South China Sea due to orographic wind jets. *J. Phys. Oceanogr.*, **38**, 726–732, https://doi.org/10.1175/2007JPO3868.1.

Wang, J., and C.-S. Chern, 1987: The warm-core eddy in the northern South China Sea. I. Preliminary observations on the warm-core eddy (in Chinese with English abstract). *Acta Oceanogr. Taiwan*, **18**, 92–103.

Wang, Y., G. Fang, Z. Wei, F. Qiao, and H. Chen, 2006: Interannual variation of the South China Sea circulation and its relation to El Niño, as seen from a variable grid global ocean model. *J. Geophys. Res.*, **111**, C11S14, https://doi.org/10.1029/2005JC003269.

Wu, C.-R., 2012: Interannual modulation of the Pacific Decadal Oscillation (PDO) on the low-latitude western North Pacific. *Prog. Oceanogr.*, **110**, 49–58, https://doi.org/10.1016/J.POCEAN.2012.12.001.

——, and T.-L. Chiang, 2007: Mesoscale eddies in the northern South China Sea. *Deep-Sea Res. II*, **54**, 1575–1588, https://doi.org/10.1016/j.dsr2.2007.05.008.

——, and Y.-C. Hsin, 2012: The forcing mechanism leading to the Kuroshio intrusion into the South China Sea. *J. Geophys. Res.*, **117**, C07015, https://doi.org/10.1029/2012JC007968.

——, Y.-L. Wang, Y.-F. Lin, T.-L. Chiang, and C.-C. Wu, 2016: Weakening of the Kuroshio intrusion into the South China Sea under the global warming hiatus. *IEEE J. Sel. Top. Appl. Earth Obs. Remote Sens.*, **9**, 5064–5070, https://doi.org/10.1109/JSTARS.2016.2574941.

——, ——, ——, and S.-Y. Chao, 2017: Intrusion of the Kuroshio into the south and East China Seas. *Sci. Rep.*, **7**, 7895, https://doi.org/10.1038/s41598-017-08206-4.

Xiu, P., and F. Chai, 2011: Modeled biogeochemical responses to mesoscale eddies in the South China Sea. *J. Geophys. Res.*, **116**, C10006, https://doi.org/10.1029/2010JC006800.

——, M. Guo, L. Zeng, N. Liu, and F. Chai, 2016: Seasonal and spatial variability of surface chlorophyll inside mesoscale eddies in the South China Sea. *Aquat. Ecosyst. Health Manage.*, **19**, 250–259, https://doi.org/10.1080/14634988.2016.1217118.

Xue, H., F. Chai, N. Pettigrew, D. Xu, M. Shi, and J. Xu, 2004: Kuroshio intrusion and the circulation in the South China Sea. *J. Geophys. Res.*, **109**, C02017, https://doi.org/10.1029/2002JC001724.

Yang, Q., H. Liu, and P. Lin, 2020: The effect of oceanic mesoscale eddies on the looping path of the Kuroshio intrusion in the Luzon Strait. *Sci. Rep.*, **10**, 636, https://doi.org/10.1038/s41598-020-57487-9.

Yu, K., and T. Qu, 2013: Imprint of the Pacific Decadal Oscillation on the South China Sea throughflow variability. *J. Climate*, **26**, 9797–9805, https://doi.org/10.1175/JCLI-D-12-00785.1.

Yuan, D., and Z. Wang, 2011: Hysteresis and dynamics of a western boundary current flowing by a gap forced by impingement of mesoscale eddies. *J. Phys. Oceanogr.*, **41**, 878–888, https://doi.org/10.1175/2010JPO4489.1.

Zhang, M., Y. Li, W. Wang, and Q. Huang, 1995: A three dimensional numerical circulation model of the South China Sea in winter. *Proc. Symp. Marine Sciences in Taiwan Strait and Its Adjacent Waters*, Beijing, China, China Ocean Press, 73–82.

Zhang, Z., W. Zhao, J. Tian, and X. Liang, 2013: A mesoscale eddy pair southwest of Taiwan and its influence on deep circulation. *J. Geophys. Res. Oceans*, **118**, 6479–6494, https://doi.org/10.1002/2013JC008994.

——, ——, ——, Q. Yang, and T. Qu, 2015: Spatial structure and temporal variability of the zonal flow in the Luzon Strait. *J. Geophys. Res. Oceans*, **120**, 759–776, https://doi.org/10.1002/2014JC010308.

——, J. Tian, B. Qiu, W. Zhao, P. Chang, D. Wu, and X. Wan, 2016: Observed 3D structure, generation, and dissipation of oceanic mesoscale eddies in the South China Sea. *Sci. Rep.*, **6**, 24349, https://doi.org/10.1038/srep24349.

——, W. Zhao, B. Qiu, and J. Tian, 2017: Anticyclonic eddy sheddings from Kuroshio loop and the accompanying cyclonic eddy in the northeastern south China sea. *J. Phys. Oceanogr.*, **47**, 1243–1259, https://doi.org/10.1175/JPO-D-16-0185.1.

Zhao, R., and X. Zhu, 2016: Weakest winter South China Sea western boundary current caused by the 2015–2016 El Niño event. *J. Geophys. Res. Oceans*, **121**, 7673–7682, https://doi.org/10.1002/2016JC012252.

Zhao, Y.-B., X. S. Liang, and J. Gan, 2016: Nonlinear multiscale interactions and internal dynamics underlying a typical eddy-shedding event at Luzon Strait. *J. Geophys. Res. Oceans*, **121**, 8208–8229, https://doi.org/10.1002/2016JC012483.

Zheng, Q., C.-R. Hu, L. Xie, and M. Li, 2019: A case study of a Kuroshio main path cut-off event and impacts on the South China Sea in fall-winter 2013–2014. *Acta Oceanol. Sin.*, **38**, 12–19, https://doi.org/10.1007/s13131-019-1411-9.

Zhou, C., W. Zhao, J. Tian, X. Zhao, Y. Zhu, Q. Yang, and T. Qu, 2017: Deep western boundary current in the South China Sea. *Sci. Rep.*, **7**, 9303, https://doi.org/10.1038/s41598-017-09436-2.